北京航空航天大学优秀研究生校长奖学金申请表

姓名	朱丰年	学号	ZY1710226	性别	男	政治面貌	共青团员		
专业	生物医学工程			导师	李萍	入学年月	2017.9	民族	汉

申请奖学金类别：

☑优秀研究生海外游学与实践奖学金　□研究生科技竞赛奖学金

□优秀研究生社会公益奖学金　□ 优秀学生干部奖学金

在读期间的思想政治表现	（非党员、非团员无需填写此栏） 朱丰年同学态度端正，积极进取，思想政治觉悟较高。同意。 党（团）支部书记签字　杨水寿　2019年　3月　7　日
	指导主任（副书记）签字　　　　年　　月　　日

主要申请理由（简述）

1、研究生期间成绩单（另附）

2、在读期间发表的论文以及论文级别

1）《Advanced Energy Materials》 文章已接收，附邮件证明

2）《Small》 发表日期：2019-1-15 文章另附

3、在读期间主要工作成绩（根据申报类别重点表述）

1）2019 秋季北航-比利时列日大学交换生项目；

2）雅思 6.0；

3）2018 北航国际研究生暑期学校优秀学员；

4） 远航伙伴志愿者。

4、获奖情况：

本人签字　朱丰年　2019年　3月　7　日

导师意见

1、　该研究生提供的材料是否属实。　是 ☑　否 □

2、　您对研究生的学术、科研能力的评价。　优秀 ☑　比较优秀 □　一般 □

3、　您对推荐该研究生获得该项奖学金的意见。　同意 ☑　一般同意 □　不同意 □

导师签字　2019 年 3 月 8 日

学院评审委员会意见

评审委员会组长签字（盖章）　年　月　日

校评审委员会审批意见 盖章　年　月　日	备注

注：该表最长不超过 2 页，A4 纸正反面打印。发表论文必须注明发刊号、发表日期，否则按没有发表处理。发表论文以及获奖情况另附复印件。在读期间主要工作成绩一栏：申请者主要填写符合相关奖项的成绩及事迹。

研究生事迹

生物与医学工程学院 朱丰年 ZY1710226

来到北航已有一年多啦，刚入学那会的憧憬随着时间的带过逐渐蔓延开来，开始我对于研究生是有一些好奇的，这种好奇不同于刚进本科那会，刚从封闭式的高中进入开放的大学。对于研究生，很多人都说过，这个环境会更加的开放，需要开展自己的课题，需要敢于探索，所以带着好奇对未知的寻找成了我研究生期间的主旋律。开学典礼是我来北航的第一课，徐校长自信而幽默的演讲点燃了我的热情，始终忘不的一句话是“理想高远、学识一流、胸怀寰宇、致真唯实”，这个条幅也在学二食堂挂过一段时间，每每我在吃饭的时候，晚上从图书馆回宿舍的时候都会想想这句话，远望星空的追求、容纳万物的博大心胸、脚踏实地的勤奋致学，这句话也成为我在北航的座右铭，开启了在这里的生活。

一、学习和科研

研究生第一学年主要是上课，修满足够的学分，和导师商量后选择了合适的专业课程，挑选了自己感兴趣的公共课，经过一番努力后，课程全部通过，拿到足够的课程学分。在上课之余，从研一上学期开始进入实验室，尝试过静电纺丝、氧化铁纳米颗粒合成以及导电聚合物的合成，这一系列的尝试帮助我很好的适应了科研环境，了解各种实验仪器，和师兄师姐建立了很好的关系。到了研二上学期，调整我的实验思路，经过阅读文献以及与老师探讨后，决定利用磁性纳米颗粒载药进行癌症治疗，这既是一个趋势也是一个挑战。经过半年多的打磨，实验思路也越来越清晰，现在正处于实验的关键阶段。在科研论文方面，本科期间的毕业设计关于金属有机框架应用于超级电容器，取得了很好的效果，作为共同作者发表在《Advanced Energy Materials》和《Small》上。

二、研究生活动

开学时，有许多社团和部门开始纳新，我选择了本学院的文体部，希望能认识到一些新的朋友，接触到一些新鲜的事。刚进去的时候，学校举办了研究生运

动会，这成为了我们部门增进感情的契机，从招募远动员，到组织训练，再到比赛的安排与后勤，我们均很好的完成了任务，提升了自己。同样的团队，到了学院元旦晚会和院庆晚会又站在了一起，我主要负责舞台灯光操作，互相的团结配合，取得了很好的效果。

此外，我还参加了 2018 北航国际研究生暑期学校和北航 Buddy 计划，与他们进行学术交流，介绍彼此的文化，帮助他们融入北航的生活，起到很好的交流作用，体验到很多新鲜的事物。

三、业余活动

我的业余爱好非常丰富，这些业余活动帮助我认识了许多朋友，增进了我们的感情。特别喜欢足球，作为院队的一员在绿茵场上和兄弟们一起拼搏的感受很好。喜欢旅游和徒步，让我的视野更加开阔，更加清楚探索的目的。其它业余时间，我也会去骑车、游泳和爬山，劳逸结合以便让自己处在高效率状态，使研究生的生活更加充实。

四、关于出国

我选择 2019 秋季北航-比利时列日大学交换生项目的原因有三。其一：出去交流能给我更广阔的平台、更开阔的视野，这是我选择这个项目最根本的原因。要想成为一名优秀的科研工作者，必须要到国际上的舞台去锻炼，去和不同的人交流，掌握新的技能，交换生项目能够很好的帮助我达到这些，或许能够帮助我开辟一条不一样的人生方向。其二：列日大学位于欧洲，学术氛围和课程结构对于我来说充满着吸引力，在那里我相信一定能收获很多。其三：思维和文化交流的吸引力， 在 2018 年北航国际研究生暑期学校（IGSS）项目中，我结识了两位非常好的朋友 Niklas 和 Adnan，我们进行了学术和文化上的深入交流，共同想出了利用无人机清理北京雾霾的点子，对他们的思维想法感到非常新鲜，这种多领域思维交流给了我们很大的愉悦感和满足感。另外，我们分享彼此的文化，带他们领略中华文明的博大精深，在短短的几天里，我们结下了非常深厚的友谊，这段美妙的旅程给了我参加这个项目很大的推动力。

研究生生涯已经过半，过得充实且丰富多彩，非常感谢我遇到的机会与挑战。在接下来的一半时间里，我希望更加努力的向前，始终保持这种好奇心去探索下去。

北京航空航天大学
研究生课程成绩单

姓　　名：朱丰年　　性　　别：男
学　　号：ZY1710226　　上报学号：100062017S02464
院系名称：生物与医学工程学院　　学生类型：硕士
专业名称：生物医学工程

课程类别	课程名称	学时	学分	成绩	考试时间
必修	中国特色社会主义理论与实践研究	36	2	86	2018-01-17
必修	自然辩证法概论	18	1	80	2018-07-01
必修	英语一外（硕）	90	2	85	2018-06-21
必修	数理统计B	48	3	67	2018-01-16
必修	人文专题课：经济学思想	18	1	通过	2017-12-07
必修	高级解剖生理学	48	3	83	2017-12-31
必修	生物医学仪器分析	48	3	85	2017-12-14
必修	生物医用材料	32	2	93	2018-04-23
必修	植介入医疗器械与人工器官	32	2	90	2017-11-15
必修	组织工程与再生医学	32	2	87	2018-06-21
必修	生理信号检测与处理实验	18	1	92	2018-06-08
必修	医学图像处理及成像技术实验	18	1	87	2018-07-01
必修	人体工效学及康复工程实验	18	1	89	2018-07-16

备注：优--90分及以上；良--80～89分；中--65～79分；及格--60～64分；不及格--59分及以下；通过--60分及以上。

总学分：24　　学位课学分：24　　学位课门数：13　　选修课门数：

2018/11/2
（盖院系教务公章）

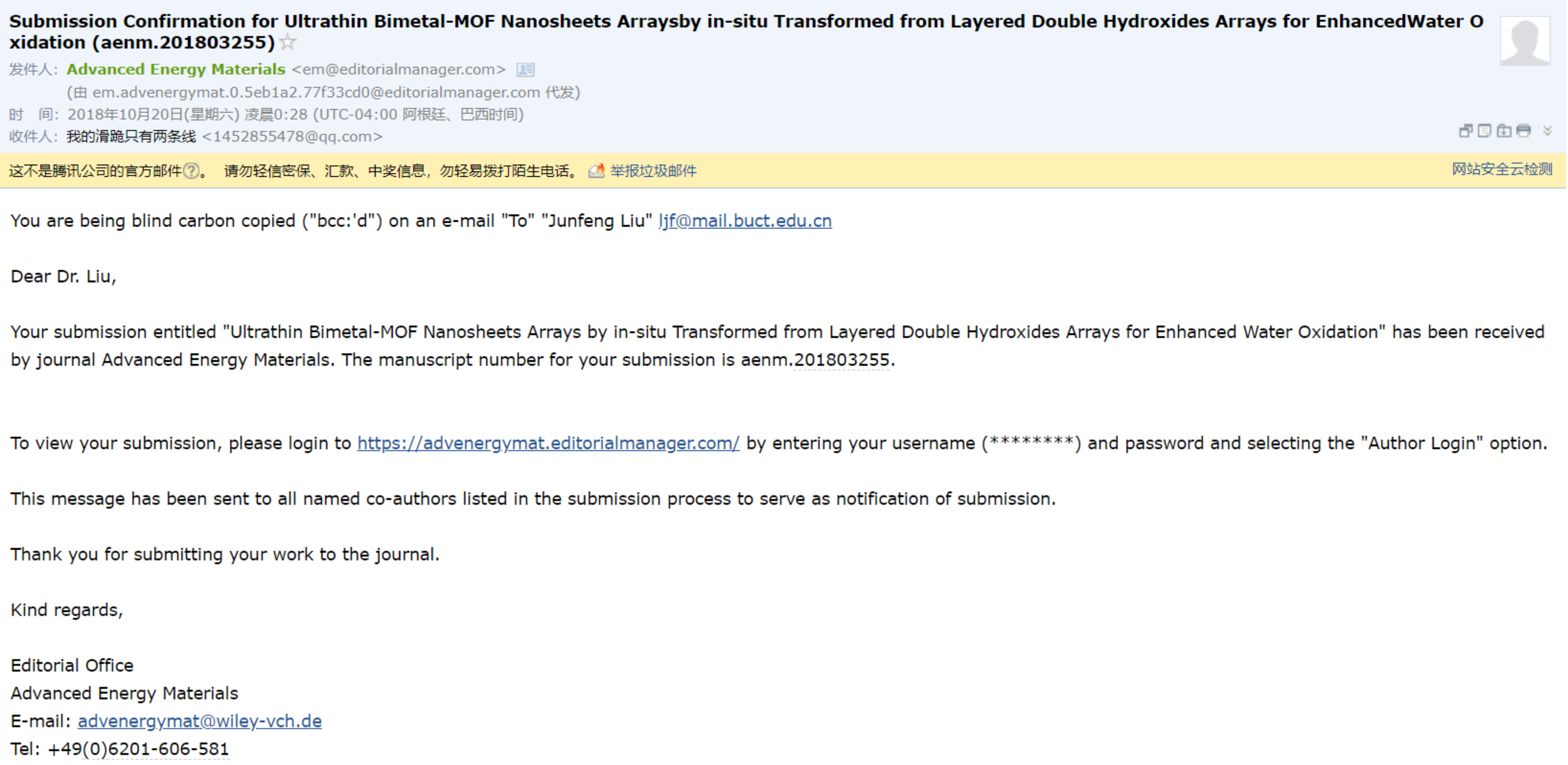

Submission Confirmation for Ultrathin Bimetal-MOF Nanosheets Arraysby in-situ Transformed from Layered Double Hydroxides Arrays for EnhancedWater Oxidation (aenm.201803255) ☆

发件人：**Advanced Energy Materials** <em@editorialmanager.com>
(由 em.advenergymat.0.5eb1a2.77f33cd0@editorialmanager.com 代发)
时　间：2018年10月20日(星期六) 凌晨0:28 (UTC-04:00 阿根廷、巴西时间)
收件人：我的滑跪只有两条线 <1452855478@qq.com>

这不是腾讯公司的官方邮件?。 请勿轻信密保、汇款、中奖信息，勿轻易拨打陌生电话。 举报垃圾邮件 网站安全云检测

You are being blind carbon copied ("bcc:'d") on an e-mail "To" "Junfeng Liu" ljf@mail.buct.edu.cn

Dear Dr. Liu,

Your submission entitled "Ultrathin Bimetal-MOF Nanosheets Arrays by in-situ Transformed from Layered Double Hydroxides Arrays for Enhanced Water Oxidation" has been received by journal Advanced Energy Materials. The manuscript number for your submission is aenm.201803255.

To view your submission, please login to https://advenergymat.editorialmanager.com/ by entering your username (********) and password and selecting the "Author Login" option.

This message has been sent to all named co-authors listed in the submission process to serve as notification of submission.

Thank you for submitting your work to the journal.

Kind regards,

Editorial Office
Advanced Energy Materials
E-mail: advenergymat@wiley-vch.de
Tel: +49(0)6201-606-581

NANO · MICRO small
www.small-journal.com

A General Method to Ultrathin Bimetal-MOF Nanosheets Arrays via In Situ Transformation of Layered Double Hydroxides Arrays

Bingqing Wang, Jing Shang, Chong Guo, Jianze Zhang, Fengnian Zhu, Aijuan Han, and Junfeng Liu**

Structure engineering of ultrathin metal–organic framework (MOF) nanosheets to self-supporting and well-aligned MOF superstructures is highly desired for diverse applications, especially important for electrocatalysis. In this work, a facile layered double hydroxides in situ transformation strategy is developed to synthesize ultrathin bimetal-MOF nanosheets (BMNSs) arrays on conductive substrates. This approach is versatile, and applicable to obtain various BMNSs or even trimetal-MOF nanosheets arrays on different substrates. As a proof of concept application, the obtained ultrathin NiCo-BDC BMNSs array exhibits an excellent catalytic activity toward the oxygen evolution reaction with an overpotential of only 230 mV to reach a current density of 10 mA cm^{-2} in 1 M KOH. The present work demonstrates a strategy to prepare ultrathin bimetal-MOF nanosheets arrays, which might open an avenue for various promising applications of MOF materials.

Metal–organic frameworks (MOFs), a new class of porous materials formed by self-assembly of metal ions and organic ligands, have been widely studied in gas storage and separation,[1] sensing,[2] catalysis,[3] etc., owing to their large surface area, ordered pore structure, abundant intrinsic molecular metal sites, as well as chemical tunability. Given these unique properties, they are also promising for electrocatalysis by choosing the suitable composition and functionality.[4] However, because of the poor electron transfer efficiency and strong diffusion resistance in bulk crystalline MOFs, only a small portion of their abundant metal sites can be utilized in electrocatalytic reactions, which restricts their performance in energy-related applications.[5] Very recently, ultrathin bimetal-MOF nanosheets (BMNSs) are emerging as highly efficient electrocatalysts for oxygen evolution reaction (OER).[5b,6] The ultrathin structure of MOF nanosheets (NSs) makes most of the active metal sites available to the reactants, which endows them with better catalytic activities compared with their bulk counterparts.[7] Unfortunately, the easy restacking nature and relatively inferior electrical conductivity of the MOF NSs limit their electrocatalytic activity far from practical applications. In addition, time-consuming coating procedures are always needed to attach powdered MOF NSs onto the surface of the electrode with the assistance of polymeric binders, which may decrease their original activity and cause mechanical stability problems.

To address these issues, one effective and feasible way is directly growing the ultrathin BMNSs on self-supported 3D macroporous conductive substrates. In this kind of hierarchical structure, first, the oriented and close arrangement of the ultrathin MOF NSs can avoid the restacking and guarantee the fully exposed electroactive sites. Second, the hierarchical pore structure of the electrode can not only enhance the mass transfer but also facilitate bubble dissipating in gas-generated reactions.[8] Moreover, the close and strong binding of ultrathin MOF NSs with the underlying conductive support gains more efficient electron transfer between them and guarantees the ultrahigh structural stability of the electrodes.[5a,9] However, until now, the controllable growth of different ultrathin BMNSs on various conductive substrates, especially the chemical inert substrates (such as carbon cloth (CC) and carbon fiber paper (CFP)), still remains a challenge because there are only few nucleation sites on the substrates and MOFs tend to form bulk crystals under conventional synthetic conditions.[10] Therefore, it is of great significance to develop a general and effective synthesis strategy to directly grow different ultrathin BMNSs on various conductive substrates to accelerate the practical application of MOFs in electrocatalysis.

Herein, we report a general strategy to synthesize various ultrathin BMNSs arrays on different conductive substrates through the in situ transformation of presynthesized layered double hydroxides (LDHs) NSs arrays, which provide an appropriate dissolution rate of metal ions in a mixed solvent. This strategy with LDHs as precursor is adaptable to bimetal-MOFs with different organic ligands and metal ions (such as NiCo-BDC (BDC = 1,4-dicarboxybenzene), NiCo-NDC (NDC = naphthalene-2,6-dicarboxylic acid), NiCo-TDA (TDA = 2,5-thiophenedicarboxylic acid), ZnCo-BDC BMNSs) on various substrates (such as nickel foam (NF), CC, and CFP, benefiting from the multimetal tunability and flexibility of LDHs. In addition, trimetal-MOF NSs

---

B. Wang, J. Shang, C. Guo, J. Zhang, F. Zhu, Dr. A. Han, Prof. J. Liu
State Key Laboratory of Chemical Resource Engineering
Beijing University of Chemical Technology
Beijing 100029, P. R. China
E-mail: hanaijuan@mail.buct.edu.cn; ljf@mail.buct.edu.cn

The ORCID identification number(s) for the author(s) of this article can be found under https://doi.org/10.1002/smll.201804761.

DOI: 10.1002/smll.201804761

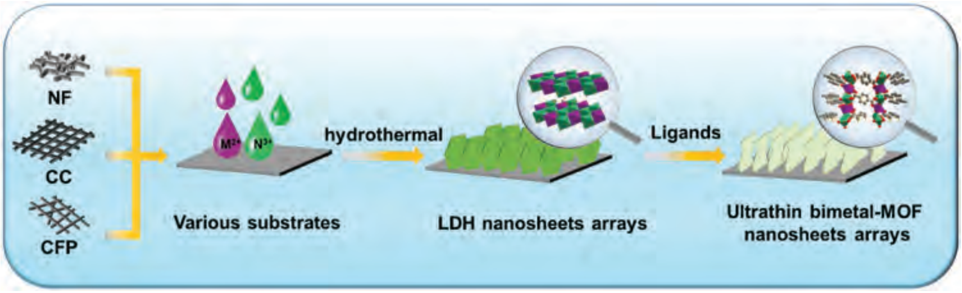

Figure 1. Schematic illustration showing the fabrication of ultrathin BMNSs arrays on the 3D conductive matrix.

(TMNSs), such as ultrathin NiCoCu-BDC TMNSs array, can also be achieved when using ternary NiCoCu-LDH NSs array as the precursor, demonstrating the versatility of the approach. The obtained ultrathin BMNSs array shows good performance, taking NiCo-BDC BMNSs array as an example, which exhibits better activity and durability toward OER than other NiCo-based counterparts due to the excellent 3D construction of the nanoarray with fast ion diffusion, efficient charge transfer, and more exposed active sites.

The synthetic process for the ultrathin BMNSs arrays involves a two-step growth procedure, as shown in **Figure 1**. LDH NSs array was first grown onto 3D substrates. Then, the obtained LDH NSs array was in situ transformed into BMNSs array through a solvothermal step. In this step, LDH NSs array not only acts as self-templates to form the ultrathin array structure, but also works as self-sacrificial precursors to provide metal ions for BMNSs growth, in which they were dissolved with the assistance of solvents and ligands. NiCo-LDH NSs array on NF (**Figure 2**a; Figure S1, Supporting Information) was first chosen as the precursor to prepare NiCo-based ultrathin BMNSs arrays. In a typical experiment, the NiCo-LDH NSs array was immersed into 4 mL of mixed solvent of N,N-dimethylformamide (DMF) and deionized (DI) water, which containing a certain amount of BDC as ligand, and then maintained at 100 °C for 24 h. The deprotonated H^+ from the BDC gradually reacts with NiCo-LDH NSs and releases nickel and cobalt species. The released metal ions in situ coordinated with the BDC ligands to form ultrathin NiCo-BDC BMNSs until the NiCo-LDH NSs were exhausted. After the transformation, the resultant product exhibits a hierarchical structure with ultrathin BMNSs interconnected with each other, forming a highly open 3D network (Figure 2b; Figure S2, Supporting Information). Typical reflections of (00*l*) are shown in the X-ray diffraction (XRD) pattern of the pristine NiCo-LDH NSs,[11] which totally disappears after 24 h conversion (Figure 2c). Instead, strong diffraction peaks isostructural to the Ni-based MOF (No. 985 792, $Ni_2(OH)_2(C_8H_4O_4)$, Cambridge Crystallographic Data Centre)[6,12] are observed, testifying the successful transformation of NiCo-LDH NSs to NiCo-BDC BMNSs. The transmission electron microscopy (TEM) image of the NiCo-BDC BMNSs detached from NF substrate shows their low contrast (Figure 2d). The selected area electron diffraction (SAED) pattern collected from an individual NiCo-BDC BMNS shows diffraction spots attributed to the (200), ($\bar{2}01$), and (001) planes (Figure 2d, inset), which agrees well with the simulated ones along the [010] axis, confirming their crystal structure and single crystallinity (Figure S3, Supporting Information). The lattice spacing of 1.01 nm corresponding to the (200) plane of NiCo-BDC is also clearly observed in a typical high-resolution TEM (HRTEM) image (Figure 2e). Atomic force microscopy (AFM) is taken to further determine the thickness. NiCo-BDC BMNSs exhibit only about 5 nm thickness, revealing the ultrathin nature (Figure 2f). The thickness of the generated MOF NSs could be well controlled by regulating the DI water amount in the mixed solvent, the metal ions dissolution rate of the LDH precursor is adjustable in the mixed solvent of DMF and DI water. As shown in Figure 1g,h, the thicknesses of the obtained MOF sheets are about several dozens and several hundred nanometers when using the mixed solvent of DMF:H_2O = 6:1 and 4:1, respectively, indicating that higher DMF to DI water ratio will lead to thinner MOF sheets. However, further increasing the DMF:H_2O ratio from 10:1 to 12:1 showed no obvious influence on the thickness of the generated BMNSs, but the LDHs precursor cannot fully convert to BMNSs as indicated by XRD investigation (Figure S4, Supporting Information). In addition, no transformation occurs without DI water in the reaction solvent, demonstrating the important role of water in the dissolution of LDHs to release the metal ions for MOF nanosheets growth. Energy dispersive X-ray spectroscopy (EDS) maps indicate uniform spatial distributions of Ni, Co, C elements in the NiCo-BDC BMNSs (Figure 2i–l). In addition, the quantitative measurement by inductively coupled plasma-mass spectrometry reveals that the atomic ratio of Ni and Co in NiCo-BDC BMNSs was 2.3:1, in consistence with the EDS result (Figure S5, Supporting Information). Furthermore, the well-aligned ultrathin BMNSs array exhibits a superhydrophilic surface (Figure S6, Supporting Information), which could offer much abundant high electrode/electrolyte interface for electrocatalytic reactions.

To further confirm the successful transformation of the NiCo-LDH NSs to NiCo-BDC BMNSs, the Fourier transform infrared spectroscopy (FTIR) and Brunauer–Emmett–Teller measurements were performed. The FTIR spectrum of pristine NiCo-LDH NSs in **Figure 3**a shows the peaks centered at 3461, 1616, and 1054 cm^{-1} deriving from the vibrations of the interlayer free OH, water molecules, and methanol molecules, respectively.[11] After reacting with BDC for 24 h, the peaks belonged to LDH disappeared and several new peaks arose. The new bands located at 3595 and 1504 cm^{-1} can be attributed to the stretching vibrations of OH^- and paraaromatic C—H groups in NiCo-BDC ($Ni_{2.3}Co(OH)_2(C_8H_4O_4)$) BMNSs,[13] respectively. Besides, another two new bands at 1581 and 1377 cm^{-1}, assigned to the $\nu_{as}(-COO^-)$ and $\nu_s(-COO^-)$, are slightly shifted compared to the pure BDC, proving the successful

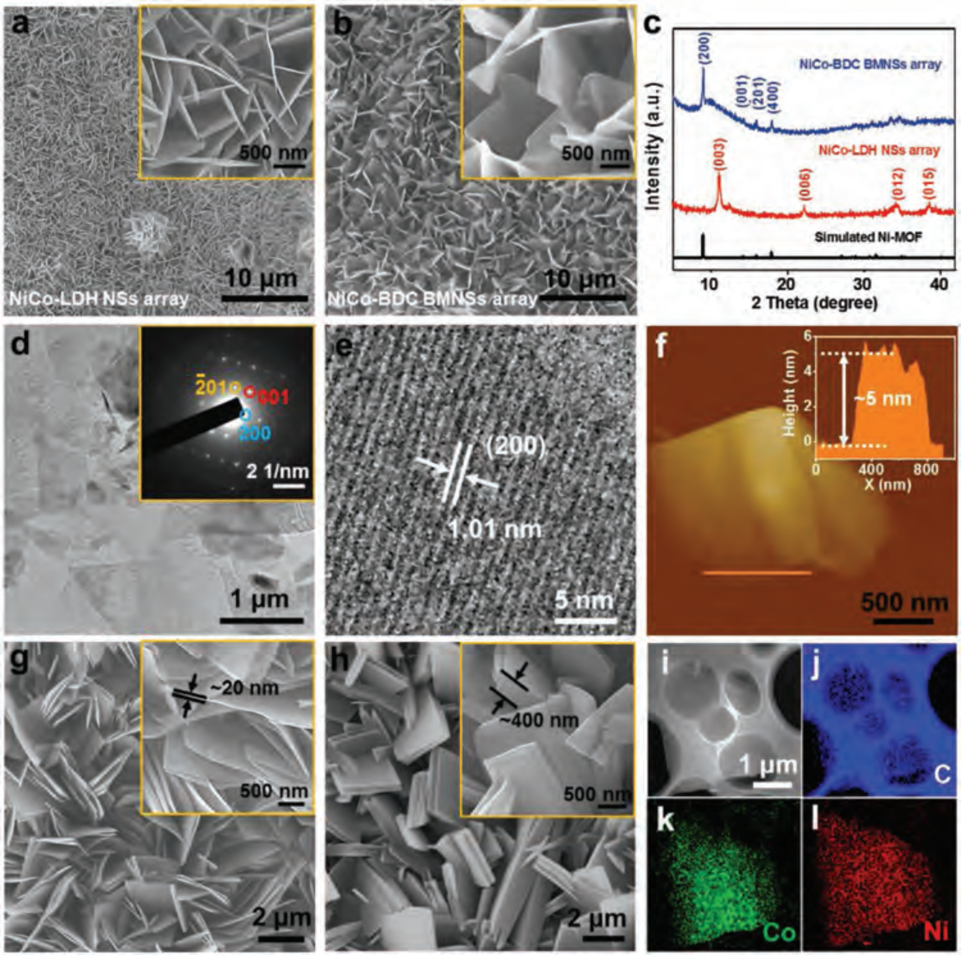

Figure 2. Morphological and phase characterization of NiCo-BDC BMNSs array. SEM images of a) NiCo-LDH NSs and b) NiCo-BDC BMNSs arrays (the inset shows the high magnification SEM images). c) XRD patterns of NiCo-BDC BMNSs array and pristine NiCo-LDH NSs array. d) TEM, e) HRTEM, f) AFM images and i–l) EDX mapping of NiCo-BDC BMNS. SEM images of NiCo-BDC BMNSs with different thickness synthesized at g) DMF:H_2O = 6:1 and h) DMF:H_2O = 4:1 (the inset shows the high magnification SEM images) (inset of (d): the SAED pattern of a single BMNS; inset of (f): the corresponding height profle measured along the yellow line).

coordination of metal ions with the linker molecules.[14] Moreover, the specific surface area of NiCo-BDC BMNSs is 50.8 m^2 g^{-1}, which is about two times that of the pristine NiCo-LDH NSs (24.9 m^2 g^{-1}) (Figure 3b). The obtained ultrathin NiCo-BDC BMNSs array with the high surface area will be favorable for the accessibility of electrolyte and provide additional active sites for electrocatalysis. Additionally, X-ray photoelectron spectroscopy (XPS) was employed to investigate the surface electronic state change after transformation. The survey spectra indicate that NiCo-BDC BMNSs contain Ni, Co, C, and O elements without other impurities (Figure S7, Supporting Information), consistent with the EDS analysis. In the high-resolution Ni 2p and Co 2p XPS spectra of NiCo-BDC BMNSs, the fitted curves show the main peaks for two kinds of nickel species of Ni^{2+} and Ni^{3+}, as well as two kinds of cobalt species of Co^{2+} and Co^{3+}, which well inherit the valance state in pristine NiCo-LDH NSs (Figure 3c,d). It interprets that NiCo-LDH NSs act as the metal source to provide the metal ions in the in situ transformation to bimetal-MOFs. Compared with the XPS peaks of pristine NiCo-LDH NSs, Ni 2p and Co 2p peaks of NiCo-BDC BMNSs slightly shift to higher binding energy due to the coordination between Ni or Co species and BDC ligands, which draws electrons from the metal species.[15] Such strong electronic interactions could benefit the electrocatalytic oxidation activity.[15b,16]

The present strategy with LDH NSs array as precursors possesses several advantages, making it versatile for the synthesis of different BMNSs on various substrates. 1) By regulating the immersing solvent of LDH NSs array, the growth of BMNSs can be well controlled, making it possible to form ultrathin NSs array of various bimetal-MOFs. As shown in **Figure 4**a,b and Figure S8a,b (Supporting Information), the ultrathin NiCo-NDC and NiCo-TDA BMNSs arrays were successfully fabricated by replacing BDC with NDC and TDA. 2) Benefiting from the multimetal tunability and flexibility of LDHs, this strategy is easy to apply to synthesize other binary- or ternary-metal MOF NSs arrays. For instance, the ZnCo-BDC BMNSs or NiCoCu-BDC TMNSs arrays were achieved by using the ZnCo-LDH or NiCoCu-LDH NSs array as the precursors, respectively (Figure 4c,d; Figures S8c–f and S9, Supporting Information). 3) The growth of BMNSs arrays on different substrates, which

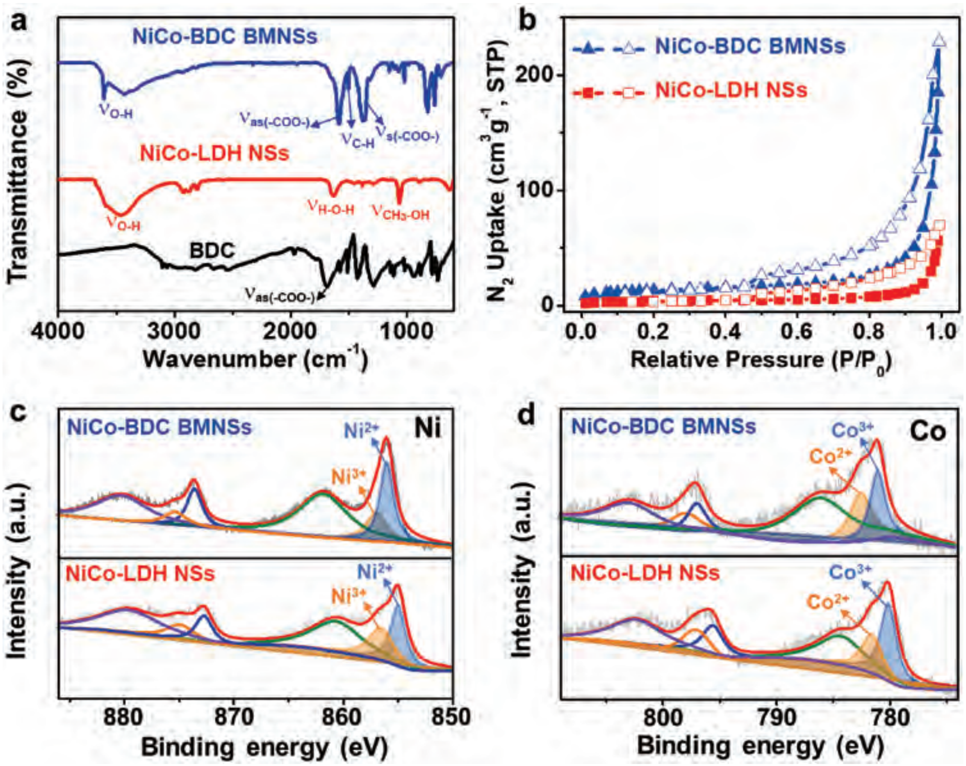

Figure 3. FTIR spectra, N_2 sorption isotherms, and XPS spectra. a) FTIR spectra, b) N_2 adsorption–desorption isotherms (77 K), and c) high-resolution Ni 2p and d) Co 2p XPS spectra of NiCo-BDC BMNSs compared to NiCo-LDH NSs.

is highly desirable for diverse applications, can also be easily achieved, since the synthesis of LDHs nanoarray with diverse chemical compositions on various substrates has been widely studied.[17] By using NiCo-LDH NSs arrays on CC and CFP as precursors (Figure S10, Supporting Information), they were successfully converted to NiCo-BDC BMNSs arrays on CC and CFP with this strategy (Figure 4e,f; Figure S11, Supporting Information). Overall, above results demonstrated that our synthetic strategy is general and effective to produce and tune the functionality of various BMNSs arrays on different substrates.

To reveal the advantages of the self-supporting and well-aligned ultrathin BMNSs superstructures, OER activity of the as-synthesized NiCo-BDC BMNSs array is investigated in 1.0 M KOH using a typical three-electrode system. The 3D self-supported electrode was used as the working electrode directly without additional binder and substrate. For comparison, the same amount of NiCo-BDC BMNSs powder detached from the NiCo-BDC BMNSs array and reloaded on NF using Nafion as the binder (denoted as NiCo-BDC BMNSs powder), pristine NiCo-LDH NSs array and IrO_2 on NF are also investigated. **Figure 5**a shows the linear sweep voltammetry (LSV) curves of all the electrodes at a scan rate of 1 mV s^{-1} with iR compensation (see the raw data of NiCo-BDC BMNSs array in Figure S12a, Supporting Information). Specifically, the NiCo-BDC BMNSs array electrode only needs overpotentials of 230 and 292 mV to drive the current densities to 10 and 100 mA cm^{-2} with a Tafel slope of 61 mV dec^{-1}, which are much lower than that of powdered NiCo-BDC BMNSs, pristine NiCo-LDH NSs array, and commercial IrO_2 (Figure 5b,c). Additionally, LSV curves with the specific mass current density (Figure S12b, Supporting Information), further demonstrate that the NiCo-BDC BMNSs array has superior electrocatalytic activity than the other samples. The NiCo-BDC BMNSs array gains much better performance than most NiCo-based OER catalysts with various configurations (Table S1, Supporting Information), further verifying its outstanding OER catalytic behavior. Considering the powdered NiCo-BDC BMNSs have the same active sites as the NiCo-BDC BMNSs arrays, therefore, the better OER performance of NiCo-BDC BMNSs array than of powdered NiCo-BDC BMNSs clearly arises from the specific structure. On one hand, the thin nanosheet array structure enables close contact with electrolyte, promotes the ion diffusion, and more importantly, results in higher number of active sites. To confirm our hypothesis, the electrochemically active surface area (ECSA) test was performed. The cyclic voltammetry measurements at different scan rates were carried out to determine the double-layer capacitance (C_{dl}), which is used to estimate the ECSA (Figure 5d; Figure S13, Supporting Information). The NiCo-BDC BMNSs array possesses the highest C_{dl} of 6.25 mF cm^{-2}, which is nearly twice that of the powdered NiCo-BDC BMNSs, indicating more exposure of the active sites in the NiCo-BDC BMNSs array. On the other hand, electron transfer between the ultrathin BMNSs and the conductive substrates is also facilitated, as indicated by a smaller charge transfer resistance of NiCo-BDC BMNSs array than the powdered NiCo-BDC BMNSs in electrochemical impedance spectra (EIS) (Figure 5e). In addition, the thickness effect of the MOF sheets on the OER activities was also investigated. The results

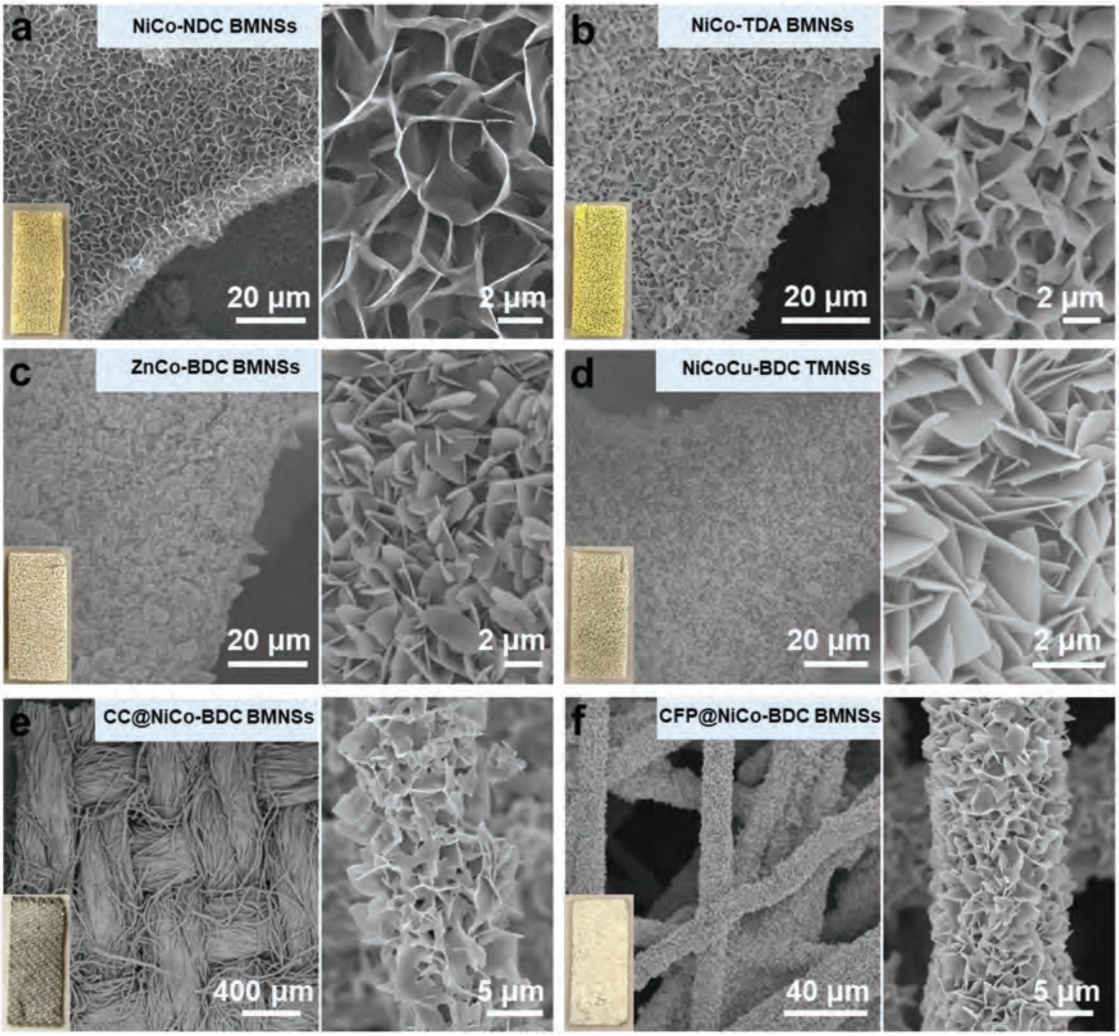

Figure 4. The general synthesis of different BMNSs arrays on various substrates. Low and high magnifation SEM images of a) NiCo-NDC BMNSs, b) NiCo-TDA BMNSs, c) ZnCo-BDC BMNSs, d) NiCoCu-BDC TMNSs arrays on NF, and NiCo-BDC BMNSs array on e) CC and f) CFP (inset of (a)–(f): the photographs of corresponding products).

showed that the thinner MOF sheets exhibited better OER performance (Figure S14, Supporting Information), which can be attributed to the higher mass and electron transfer efficiency and more metal sites[5b,6] upon the ultrathin BMNSs.

Apart from the high catalytic activity, the operating stability is also important to practical applications. Figure 5f shows the current density curves as a function of time recorded at varied potentials over 24 h for OER. No appreciable deactivation is observed for the NiCo-BDC BMNSs array electrode in this time interval, while the current density for powdered NiCo-BDC BMNSs decreased much larger at high current density (50 mA cm^{-2}). This phenomenon could be attributed to the structure destruction of powdered NiCo-BDC BMNSs electrode upon the oxygen bubble evolution during the electrochemical process, as a large amount of the catalysts falling off from the substrate could be observed in the reaction cell (Figure S15a, Supporting Information). It further testifies the mechanical stable advantage of this nanoarray structure as electrode. The scanning electron microscopy (SEM) image of electrode after stability test also confirmed the nanoarray feature preserves well (Figure S15b, Supporting Information). To further investigate the stability of the MOF crystal structure, we performed the ex situ XRD characterizations during the *i–t* test of current density at 50 mA cm^{-2}. The peaks belonged to NiCo-BDC BMNSs in the XRD pattern gradually decrease within 2 h, and broad peaks assigned to NiOOH are observed after 12 h, which indicates a layer of metal (oxy)hydroxide species is formed in situ during OER (Figure S16, Supporting Information). This kind of catalyst oxidation phenomenon is similar to that of the reported metal phosphides, sulfides, and selenides catalysts, where a layer of metal (oxy)hydroxide species was observed during OER.[18]

In summary, we have developed a general and facile LDH in situ transformation strategy to synthesize various BMNSs arrays on different conductive substrates. LDH plays a key role to obtain the BMNSs arrays, which not only acts as the precursor but also modulator to control release metal ions in situ for MOF growth. Importantly, the obtained NiCo-BDC BMNSs array can be directly used as an efficient electrode for

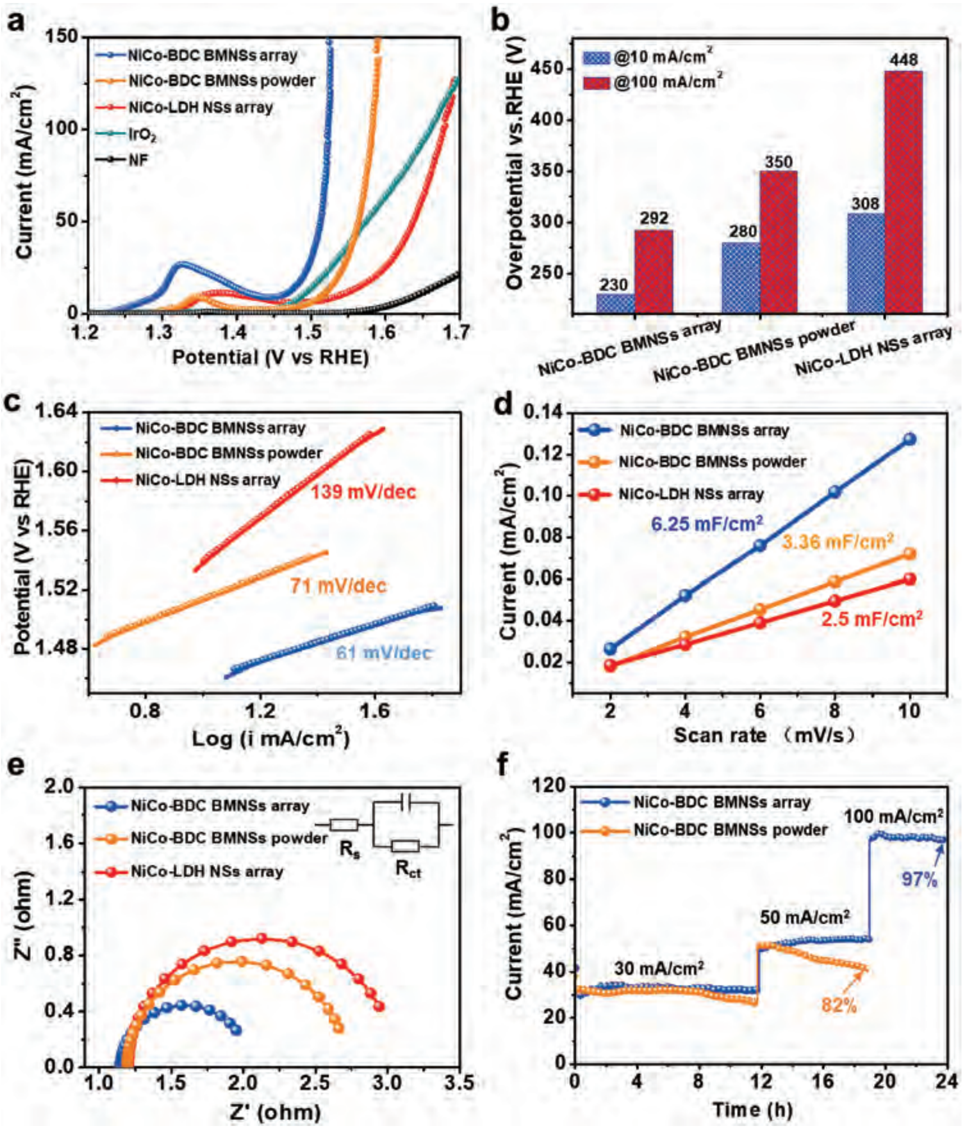

Figure 5. Electrocatalytic properties of NiCo-BDC BMNSs array for OER. a) Polarization curves, b) the overpotential comparison at the current density of 10 and 100 mA cm^{-2}, c) the corresponding Tafel plots, d) C_{dl} calculations, and e) EIS curves of NiCo-BDC BMNSs array, NiCo-BDC BMNSs powder, and NiCo-LDH NSs array. f) The stability curves of NiCo-BDC BMNSs array compared with NiCo-BDC BMNSs powder.

OER and exhibit much higher activity and stability compared to the NiCo-BDC BMNSs powder and the pristine NiCo-LDH NSs array. The high activity and stability are attributed to the unique nanoarray architecture, which enables the electrode with fast ion diffusion and charge transfer, exposed more active sites, and accelerated gas bubble release. Such a general and effective strategy to fabricate the BMNSs on the conductive substrate should be generally applicable for significantly enhancing the electrochemical performance in energy conversion and storage.

Supporting Information

Supporting Information is available from the Wiley Online Library or from the author.

Acknowledgements

This work was financially supported by the National Key Research and Development Program of China (Grant No. 2017YFA0206500), National Natural Science Foundation of China (NSFC), Beijing Natural Science Foundation (Grant No. 2172042), PetroChina Innovation Foundation, and Fundamental Research Funds for the Central Universities.

Conflict of Interest

The authors declare no conflict of interest.

Keywords

arrays, bimetal-metal–organic frameworks (MOFs), layered double hydroxides (LDHs), nanosheets, oxygen evolution reaction (OER)

Received: November 13, 2018
Revised: December 13, 2018

[1] a) T. H. Bae, J. S. Lee, W. Qiu, W. J. Koros, C. W. Jones, S. Nair, *Angew. Chem., Int. Ed.* **2010**, *49*, 9863; b) Y. He, W. Zhou, G. Qian, B. Chen, *Chem. Soc. Rev.* **2014**, *43*, 5657; c) J. L. Rowsell, E. C. Spencer, J. Eckert, J. A. Howard, O. M. Yaghi, *Science* **2005**, *309*, 1350.

[2] L. E. Kreno, K. Leong, O. K. Farha, M. Allendorf, R. P. Van Duyne, J. T. Hupp, *Chem. Rev.* **2012**, *112*, 1105.

[3] a) W. Liu, J. Huang, Q. Yang, S. Wang, X. Sun, W. Zhang, J. Liu, F. Huo, *Angew. Chem.* **2017**, *129*, 5604; b) B. Wang, W. Liu, W. Zhang, J. Liu, *Nano Res.* **2017**, *10*, 3826; c) Q. Yang, W. Liu, B. Wang, W. Zhang, X. Zeng, C. Zhang, Y. Qin, X. Sun, T. Wu, J. Liu, F. Huo, J. Lu, *Nat. Commun.* **2017**, *8*, 14429; d) M. Zhao, K. Yuan, Y. Wang, G. Li, J. Guo, L. Gu, W. Hu, H. Zhao, Z. Tang, *Nature* **2016**, *539*, 76.

[4] a) F. Li, Q. Shao, X. Huang, J. Lang, *Angew. Chem., Int. Ed.* **2018**, *57*, 1888; b) R. D. Senthil, X. Chuah, S. Lu, *Adv. Energy Mater.* **2018**, *8*, 1801065; c) J. Shen, P. Liao, D. Zhou, C. He, J. Wu, W. Zhang, J. Zhang, X. Chen, *J. Am. Chem. Soc.* **2017**, *139*, 1778; d) X. Lu, P. Liao, J. Wang, J. Wu, X. Chen, C. He, J. Zhang, G. Li, X. Chen, *J. Am. Chem. Soc.* **2016**, *138*, 8336; e) Y. Li, Y. Xu, W. Yang, W. Shen, H. Xue, H. Pang, *Small* **2018**, *14*, 1704435; f) B. Wurster, D. Grumelli, D. Hötger, R. Gutzler, K. Kern, *J. Am. Chem. Soc.* **2016**, *138*, 3623; g) P. Manna, J. Debgupta, S. Bose, S. K. Das, *Angew. Chem., Int. Ed.* **2016**, *55*, 2425.

[5] a) J. Duan, S. Chen, C. Zhao, *Nat. Commun.* **2017**, *8*, 15341; b) G. Hai, X. Jia, K. Zhang, X. Liu, Z. Wu, G. Wang, *Nano Energy* **2018**, *44*, 345; c) J. Huang, Y. Li, R. Huang, C. He, L. Gong, Q. Hu, L. Wang, Y. Xu, X. Tian, S. Liu, *Angew. Chem.* **2018**, *130*, 4722.

[6] S. Zhao, Y. Wang, J. Dong, C. He, H. Yin, P. An, K. Zhao, X. Zhang, C. Gao, L. Zhang, J. Lv, J. Wang, J. Zhang, A. M. Khattak, N. A. Khan, Z. Wei, J. Zhang, S. Liu, H. Zhao, Z. Tang, *Nat. Energy* **2016**, *1*, 16184.

[7] a) M. Zhao, Y. Wang, Q. Ma, Y. Huang, X. Zhang, J. Ping, Z. Zhang, Q. Lu, Y. Yu, H. Xu, Y. Zhao, H. Zhang, *Adv. Mater.* **2015**, *27*, 7372; b) M. Zhao, Q. Lu, Q. Ma, H. Zhang, *Small Methods* **2017**, *1*, 1600030; c) Y. Huang, M. Zhao, S. Han, Z. Lai, J. Yang, C. Tan, Q. Ma, Q. Lu, J. Chen, X. Zhang, Z. Zhang, B. Li, B. Chen, Y. Zong, H. Zhang, *Adv. Mater.* **2017**, *29*, 1700102.

[8] X. Lu, C. Zhao, *Nat. Commun.* **2015**, *6*, 6616.

[9] a) G. Cai, W. Zhang, L. Jiao, S. Yu, H. Jiang, *Chem* **2017**, *2*, 791; b) J. Zhou, Y. Dou, A. Zhou, R. Guo, M. Zhao, J. Li, *Adv. Energy Mater.* **2017**, *7*, 1602643.

[10] a) D. Tanaka, A. Henke, K. Albrecht, M. Moeller, K. Nakagawa, S. Kitagawa, J. Groll, *Nat. Chem.* **2010**, *2*, 410; b) X. Lu, L. Gu, J. Wang, J. Wu, P. Liao, G. Li, *Adv. Mater.* **2017**, *29*, 1604437.

[11] H. Chen, L. Hu, M. Chen, Y. Yan, L. Wu, *Adv. Funct. Mater.* **2014**, *24*, 934.

[12] A. Mesbah, P. Rabu, R. Sibille, S. b. Lebègue, T. Mazet, B. Malaman, M. François, *Inorg. Chem.* **2014**, *53*, 872.

[13] F. Sun, G. Wang, Y. Ding, C. Wang, B. Yuan, Y. Lin, *Adv. Energy Mater.* **2018**, *8*, 1800584.

[14] Z. Zhang, Y. Chen, S. He, J. Zhang, X. Xu, Y. Yang, F. Nosheen, F. Saleem, W. He, X. Wang, *Angew. Chem., Int. Ed.* **2014**, *53*, 12517.

[15] a) K. Rui, G. Zhao, Y. Chen, Y. Lin, Q. Zhou, J. Chen, J. Zhu, W. Sun, W. Huang, S. X. Dou, *Adv. Funct. Mater.* **2018**, *28*, 1801554; b) D. Zhu, C. Guo, J. Liu, L. Wang, Y. Du, S. Z. Qiao, *Chem. Commun.* **2017**, *53*, 10906.

[16] A. Wang, H. Xu, J. Feng, L. Ding, Y. Tong, G. Li, *J. Am. Chem. Soc.* **2013**, *135*, 10703.

[17] a) M. Shao, R. Zhang, Z. Li, M. Wei, D. G. Evans, X. Duan, *Chem. Commun.* **2015**, *51*, 15880; b) Z. Lu, X. Wu, M. Jiang, J. Wang, J. Liu, X. Lei, X. Sun, *Sci. China Mater.* **2014**, *57*, 59.

[18] a) H. Liang, A. N. Gandi, D. H. Anjum, X. Wang, U. Schwingenschlögl, H. N. Alshareef, *Nano Lett.* **2016**, *16*, 7718; b) Y. Li, H. Zhang, M. Jiang, Y. Kuang, X. Sun, X. Duan, *Nano Res.* **2016**, *9*, 2251; c) X. Xu, F. Song, X. Hu, *Nat. Commun.* **2016**, *7*, 12324; d) S. Jin, *ACS Energy Lett.* **2017**, *2*, 1937.